Analytical and Bioanalytical Chemistry (2022) 414:1857–1865
https://doi.org/10.1007/s00216-021-03816-4

RESEARCH PAPER

Co–N–C single-atom nanozymes with oxidase-like activity for highly sensitive detection of biothiols

Liping Sun[1] · Yong Yan[2] · Shuai Chen[2] · Zijue Zhou[1] · Wei Tao[2] · Chao Li[2] · Yi Feng[1] · Feng Wang[2,3]

Received: 10 October 2021 / Revised: 21 November 2021 / Accepted: 30 November 2021 / Published online: 14 January 2022

Abstract

Biothiol detection is of great importance for clinical disease diagnosis. Previous nanozyme-based colorimetric sensors for biothiol detection showed unsatisfactory catalytic activity, which led to a high detection limit. Therefore, developing new nanozymes with the high catalytic activity for biothiol detection is extremely necessary. Recently, single-atom nanozymes (SAzymes) have attracted much attention in biosensing due to their 100% atom utilization and excellent catalytic activity. Most previous works focus on the peroxidase-like activity of Fe-based SAzymes by using unstable and destructive H_2O_2 as the oxidant. It is essential to develop new SAzymes with high oxidase-like activity for biosensing to break through the limitation. Herein, Co–N–C SAzymes with high oxidase-like activity are explored. Furthermore, Co–N–C SAzymes are used as a biosensor for colorimetric detection of biothiols (GSH/Cys) based on the inhibition of thiols toward the oxidase-like activity of Co–N–C SAzymes, which showed high sensitivity with a low detection limit of 0.07 μM for GSH and 0.06 μM for Cys. Besides, the method showed good reproducibility and high selectivity against other amino acids. This work offers new insights using Co–N–C SAzymes in the biosensing field.

Keywords Cobalt single atom · Single-atom nanozymes · Oxidase-like activity · Biothiols

Introduction

Biothiols, which mainly refer to glutathione (GSH) and cysteine (Cys), are abundant in cells and play numerous cellular functions in human physiological processes [1, 2]. GSH is the redox reservoir of cells, which participates in antioxidant functions and acts as an essential mediator in many cellular functions [3, 4]. Cys is an important nonessential amino acid that synthesizes glutathione and sulfur-containing proteins in organisms [5, 6]. Abnormal levels of biothiols were associated with multiple clinical diseases, such as malignant tumors, Parkinson's disease, Alzheimer's disease, and so on [7]. Therefore, developing a sensitive biothiol detection method is necessary. Several methods have been developed for biothiol detection, such as chromatography [8, 9], electrochemical assay [10–12], fluorescence [13–15], and colorimetric assay [16–18]. Among these assays, nanozyme-based colorimetric detection has been explored widely due to its visible, fast, and low-cost characteristics [19–21]. Nevertheless, these nanozymes showed unsatisfactory catalytic activity, which led to a high detection limit. Therefore, developing new nanozymes with high catalytic activity for biothiol detection is very important.

Nanozymes, nanomaterials with enzyme-like catalytic properties, have attracted much attention for their distinctive advantages of high stability, low cost, and ease of storage. Nevertheless, nanozymes with low densities of active sites always show inferior catalytic activity. Consequently, a new class of single-atom nanozymes (SAzymes) was

Liping Sun and Yong Yan contributed equally to this work.

✉ Chao Li
lchao@hfut.edu.cn

✉ Yi Feng
fyhfut@163.com

✉ Feng Wang
fengw420@hfut.edu.cn

[1] School of Materials Science and Engineering, Hefei University of Technology, Hefei 230009, Anhui, China

[2] School of Food and Biological Engineering, Hefei University of Technology, Hefei, Anhui 230009, People's Republic of China

[3] Key Laboratory of Metabolism and Regulation for Major Diseases of Anhui Higher Education Institutes, College of Food and Biological Engineering, Hefei University of Technology, Hefei, Anhui, China

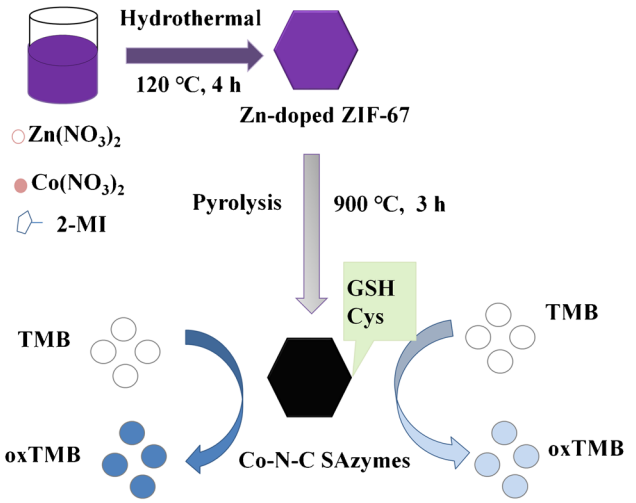

Scheme 1 Schematic illustration of Co–N–C SAzyme synthesis and colorimetric detection of GSH and Cys based on the oxidase-like activity of Co–N–C SAzymes

discovered in 2018 [22]. The atomically dispersed metal centers maximize the density of active sites and the atomic utilization efficiency [23]. Therefore, SAzymes possess remarkable enzyme-like catalytic activity compared with other nanozymes. SAzymes have been used widely in biosensing for the colorimetric detection of small molecules, such as H_2O_2 [24], ascorbic acid [25], Cr^{6+} [26], galactose [27], alkaline phosphatase (ALP) [28], acetylcholinesterase (AChE) [29], and butyrylcholinesterase (BChE) [30]. However, these detection biosensors were mainly based on the peroxidase-like catalytic activity of Fe–N–C SAzymes, which need destructive and unstable H_2O_2 as an oxidant to produce colorimetric reactions. Therefore, developing new SAzymes with high oxidase-like catalytic activity for colorimetric assays is more essential because no H_2O_2 is involved.

Herein, cobalt-based single-atom nanozymes (Co–N–C SAzymes) with exceptional oxidase-like catalytic activity were developed. Based on the phenomenon whereby biothiols tend to coordinate with metal atoms and poison the metal atom's active site, we hypothesize that Co–N–C SAzymes could be used for biothiol detection based on the inhibition of the oxidase-like activity. As illustrated in Scheme 1, we synthesized bimetallic Zn/Co metal–organic frameworks (Zn-doped ZIF-67) as a precursor, which was pyrolyzed subsequently to get uniformly dispersed Co single atoms on nitrogen-doped porous carbon (Co–N–C SAzymes) [31, 32]. Surprisingly, the obtained Co–N–C SAzymes possessed high oxidase-like activity, which oxidized colorless TMB to blue-colored oxTMB. Biothiols, such as GSH or Cys, bind to Co single atoms and inhibit oxidase-like activity, resulting in concentration-dependent color fading and absorbance decrease of the solution. Accordingly, a sensitive and straightforward colorimetric platform was developed for GSH/Cys detection with a low detection limit of 0.07 μM for GSH and 0.06 μM for Cys. We also found that this method showed high selectivity against many other common amino acids. To the best of our knowledge, this is the first report for biothiol detection based on the oxidase-like activity of Co–N–C SAzymes.

Experimental Section

Chemicals and reagents

Zinc nitrate hexahydrate was obtained from Sinopharm Chemical Reagent Co., Ltd. (Shanghai, China). Cobalt nitrate hexahydrate, methanol, 2-methylimidazole (2-MI), TMB, GSH, Cys, leucine (Leu), isoleucine (Ile), asparagine (Asn), serine (Ser), tryptophan (Trp), threonine (Thr), alanine (Ala), valine (Val), phenylalanine (Phe), glycine (Gly), lysine (Lys), and glutamic acid (Glu) were purchased from Aladdin Reagent (Shanghai, China). Fetal bovine serum (FBS) was purchased from CLARK Bioscience (USA).

Instruments

Transmission electron microscopy (TEM), high-resolution transmission electron microscopy (HRTEM), scanning transmission electron microscopy (STEM), and energy-dispersive X-ray spectroscopy (EDX) (JEM-2100F, Japan) were used to characterize the size and morphology. X-ray photoelectron spectroscopy (XPS, Thermo, USA) and X-ray powder diffraction (XRD, MAX2500VL, Japan) were performed to characterize the surface composition and bond state. Fourier transform infrared spectroscopy (FTIR, Thermo Nicolet, USA) was employed to characterize the coordination structures. The absorbance values were measured by an Infinite 200Pro microplate reader (Tecan, Switzerland). Ultraviolet–visible (UV–Vis) absorption spectra were obtained using a Lambda 465 UV/Vis spectrometer (PerkinElmer, USA).

Precursor preparation

Zn-doped ZIF-67 nanoparticles were synthesized according to previous reports [31]. Generally, 0.792 g of $Zn(NO_3)_2{\bullet}6H_2O$ and 0.038 g of $Co(NO_3)_2{\bullet}6H_2O$ were dissolved in 20 mL of methanol, which was added into 2-MI (0.876 g) in 10 mL of methanol solution and stirred at room temperature for 1 h. After that, the sample was transferred into a 100-mL Teflon-lined autoclave and heated at 120 °C for 4 h in an oven. The purple precipitate was collected by centrifugation and washed three times with methanol. The precipitate was dried overnight to get Zn-doped ZIF-67. For ZIF-67, 1.091 g of $Co(NO_3)_2{\bullet}6H_2O$ dissolved in 30 mL of methanol was mixed with 2-MI (1.231 g) in 30

mL of methanol solution. The subsequent synthetic steps were the same as those for ZIF-67. For ZIF-8, 3.56 mmol of $Zn(NO_3)_2 \bullet 6H_2O$ dissolved in 55.7 mL of methanol was mixed with 2-MI (15 mmol) in 44.3 mL of methanol solution and stirred at room temperature for 2 h. Finally, the sample was centrifuged at 14,000 rpm for 10 min, washed three times with methanol, and dried in an oven overnight to obtain ZIF-8.

Synthesis of Co–N–C SAzymes, Co Nanoparticles, and N–C Nanoparticles

The syntheses of Co–N–C SAzymes, Co nanoparticles (NPs), and N–C NPs were conducted according to previous reports [19, 31]. Generally, Zn-doped ZIF-67, ZIF-67, or ZIF-8 powder was placed into porcelain boats and transferred into a tubular furnace for pyrolysis at 900 °C for 3 h under flowing Ar gas atmosphere (heating rate 5 °C/min). After naturally cooling to room temperature, Co–N–C SAzymes, Co NPs, and N–C NPs were successfully obtained.

Oxidase-like Activity

TMB was used as the substrate for investigating the oxidase-like activity. Co–N–C SAzymes catalyzed the colorless TMB into a blue-colored oxTMB with an absorption peak at 652 nm. To compare the oxidase-like activities of Co–N–C SAzymes, Co NPs, and N–C NPs, 10 μL Co–N–C SAzymes, Co NPs, or N–C NPs (100 μg mL^{-1}) were dissolved in 90 μL acetate buffer (20 mM, pH 3), and then 1 μL TMB (25 mM) was added. After 5 min of incubation, the absorbance at 652 nm was measured by an Infinite 200Pro microplate reader. For the concentration-dependent oxidase-like activity, Co–N–C SAzymes with designated concentrations (1, 2, 5, or 10 μg mL^{-1}) were dissolved in 100 μL acetate buffer (20 mM, pH 3), after which 1 μL TMB (25 mM) was added for incubation for 5 min, and the absorbance at 652 nm was recorded. For the pH-dependent oxidase-like activity, 10 μL Co–N–C SAzymes (100 μg mL^{-1}), 1 μL TMB (25 mM), and 90 μL Milli-Q water were mixed. HCl was added to adjust the pH to 2, 3, 4, 5, 6, and 7, and NaOH was used to adjust pH to 9. The absorbance at 652 nm was recorded after 5 min of reaction. To investigate the temperature-dependent oxidase-like activity, 10 μL Co–N–C SAzymes (100 μg mL^{-1}) and 90 μL acetate buffer (20 mM, pH 3) were mixed and incubated at a temperature ranging from 25 to 75 °C for 30 min. Subsequently, 1 μL TMB (25 mM) was added.

Steady-state enzyme kinetics of Co–N–C SAzymes were assessed by varying the concentrations of TMB from 0 to 0.5 mM in acetate buffer (20 mM, pH 3). Michaelis constants (K_m) and the maximal reaction velocity (V_{max}) were calculated based on the Lineweaver–Burk plot:$1/\nu = K_m/V_{max}[S] + 1/V_{max}$, where ν corresponded to the initial velocity, K_m is the Michaelis constant, [S] is the concentration of TMB, and V_{max} means the maximal reaction velocity.

Colorimetric detection of GSH/Cys

To detect GSH/Cys, 5 μL Co–N–C SAzymes (100 μg mL^{-1}) were dissolved in 95 μL acetate buffer (20 mM, pH 3). GSH/Cys at designated concentrations (0, 0.1, 0.2, 0.4, 1, 2, 4, 10, 20, 40, 50, 100 μM) were added and incubated at 37 °C for 15 min. After that, 1 μL TMB (25 mM) was added for incubation for 5 min at room temperature. The UV–Vis spectra were recorded, and the absorbance intensity at 652 nm was used for quantitative detection of GSH/Cys. All experiments were carried out in triplicate.

For the reproducibility study, 5 μL Co–N–C SAzymes (100 μg mL^{-1}) were dissolved in 95 μL HAc/NaAc buffer (20 mM, pH 3). GSH/Cys with the final concentration of 50 μM were added and incubated at 37 °C for 15 min. After that, 1 μL TMB (25 mM) was added for incubation for 5 min at room temperature. The measurement was repeated five times.

For the selectivity study, 12 kinds of other amino acids (Leu, Ile, Asn, Ser, Trp, Thr, Ala, Val, Phe, Gly, Lys, and Glu) were used as interferences. Five microliters of Co–N–C SAzymes (100 μg mL^{-1}) was dissolved in 95 μL acetate buffer (20 mM, pH 3), and 5 μL GSH/Cys (1 mM) or 5 μL other amino acids (10 mM) were added and incubated under 37 °C for 15 min. Then, 1 μL TMB (25 mM) was added for incubation for 5 min at room temperature. The absorbance intensity at 652 nm was recorded by an Infinite 200Pro microplate reader.

Detection of GSH in biological samples

To prove the feasibility of the method in biological samples, the concentration of GSH in 10% fetal bovine serum (FBS) was measured by our method. Five microliters of Co–N–C SAzymes (100 μg mL^{-1}) were dissolved in 91 μL of 10% FBS, and 4 μL acetate buffer (500 mM, pH 3) was added to tune the pH of the solution. GSH at designated concentrations (0, 10, 20, 30, 40, 50 μM) was added and incubated at 37 °C for 15 min. Then, 1 μL TMB (25 mM) was added for incubation for 5 min at room temperature. The absorbance intensity at 652 nm was recorded by an Infinite 200Pro microplate reader.

Results and discussion

Characterization of Co–N–C SAzymes, Co NPs, and N–C NPs

Co–N–C SAzymes, Co NPs, and N–C NPs were prepared by the pyrolysis of Zn-doped ZIF-67, ZIF-67, or ZIF-8,

respectively [19, 31]. TEM images showed that Zn-doped ZIF-67, ZIF-67, and ZIF-8 possess a rhombohedral dodecahedron shape (Fig. S1). For Co–N–C SAzymes, Zn atoms were doped into ZIF-67 to separate the adjacent Co atoms. During the pyrolysis process, because of the low boiling point of Zn atoms (bp 907 °C), Zn atoms could be evaporated away, while Co could be reduced by carbonization of the organic linker, leaving isolated Co atoms anchored in the substrate. Conversely, Co NPs were obtained by calcining ZIF-67 directly without the addition of Zn atoms. Besides, N–C NPs were prepared by calcining ZIF-8, and Zn atoms were evaporated away, leaving only N–C substrate. TEM and STEM images demonstrated that Co–N–C SAzymes retained the rhombohedral dodecahedron shape after the high-temperature pyrolysis and that the average diameter of the obtained Co–N–C SAzymes was 80 nm (Fig. 1a, c). HRTEM images demonstrated layered graphitic carbon structures, and no Co nanoparticles were observed (Fig. 1b). Additionally, energy-dispersive X-ray spectroscopy (EDX) analysis (Fig. 1d) indicated that the as-prepared Co–N–C SAzymes were composed of plenty of C, N, O, and a small amount of Co element, demonstrating Co atoms were successfully doped into the carbon substrates. For Co NPs and N–C NPs, the morphology of the rhombohedral dodecahedron is shown in Fig. S2 and S3. XRD patterns of Co–N–C SAzymes and N–C NPs showed two broad diffraction peaks (Fig. 1e) corresponding to the (002) and (101) peaks of graphite carbon (PDF no. 41–1487). Notably, no crystal diffraction peaks of Co-based nanoparticles were observed for the XRD of Co–N–C SAzymes, further verifying no Co nanoparticles, which was in line with the abovementioned TEM and HRTEM images. On the contrary, the XRD patterns of Co NPs correspond with the standard characteristic peaks of cubic Co (JCPDS # 15–0806).

XPS was carried out to determine the compositions and the binding states of Co–N–C SAzymes, Co NPs, and N–C

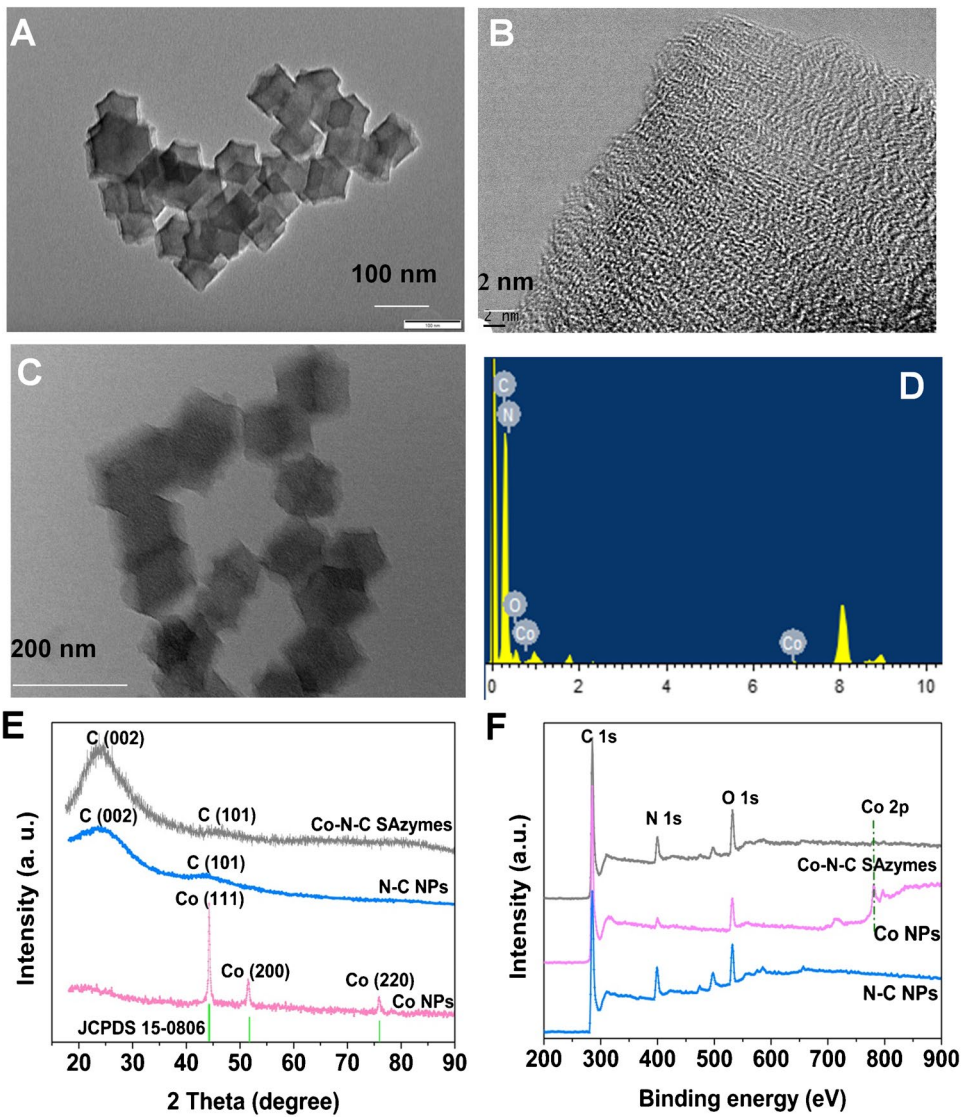

Fig. 1 **a** TEM, (**b**) HRTEM, (**c**) STEM, and (**d**) EDX energy spectrum of Co–N–C SAzymes. (**e**) XRD patterns and (**f**) XPS spectra of Co–N–C SAzymes, N–C NPs, and Co NPs

NPs (Fig. 1f). The atom percentages of C, N, O, and Co in Co–N–C SAzymes were 80.73, 9.54, 9.41, and 0.32%, respectively. The high-resolution Co 2*p* displayed four peaks at the binding energies of 780.7, 783, 796.2, and 803.7 eV, corresponding to Co $2p_{3/2}$, Co $2p_{1/2}$, Co–N, and satellite peaks, respectively. The existence of Co–N peak confirmed the coordination relationship between Co and N (Fig. 2a). The N 1*s* spectrum (Fig. 2b) of Co–N–C SAzymes was split into five peaks centered at 401.5 eV (graphite N), 398.4 eV (pyridine N), 400.7 eV (pyrrolic N), 403.8 eV (oxidized N), and 399.4 eV (Co–N). For comparison, no Co–N peak was found for Co NPs and N–C NPs. The results further confirmed that a single Co atom was anchored successfully into the N–C substrates. The high-resolution of the C 1*s* spectrum (Fig. 2c) fitted well with three peaks at the binding energies of 284.7 eV (C=C), 285.9 eV (C=N), and 288.5 eV (C–N). The binding energy of the C–N peak (288.5 eV) for Co–N–C SAzymes was 0.7 eV higher than that of Co NPs and N–C NPs (Fig. 2d), which was due to the strong electron attraction of the Co single atom in the Co–N_X moiety. The strong electron attraction of the Co single atom modified the local electronic structure, improved the electron transfer rate, and accelerated kinetics for redox reactions. All these results confirmed that isolated Co was successfully doped into the N–C framework as a single atom.

Oxidase-like activity of Co–N–C SAzymes

TMB was employed as the substrate for investigating the oxidase-like catalysis activity of Co–N–C SAzymes. As shown in Fig. 3a, Co–N–C SAzymes oxidize TMB to blue oxTMB, which showed a distinctive absorption peak at 652 nm. In contrast, neither Co NPs nor N–C NPs exhibited apparent catalytic activity toward TMB oxidation. Co–N–C SAzymes showed an 11-fold higher oxidase-like activity than Co NPs due to Co single atoms involved (Figure S4A). Furthermore, the oxidase-like activity of Co–N–C SAzymes enhanced gradually with the time increased (Fig. S4B). To investigate the role of O_2 in the reaction, the oxidase-like catalysis activity of Co–N–C SAzymes was compared in air and N_2-saturated solutions (Fig. S4C). A distinct decrease of the absorbance value at 652 nm was observed, verifying that O_2 participated in the oxidase-like catalytic reaction. The oxidase-like catalytic condition of Co–N–C SAzymes was optimized by increasing the concentrations of Co–N–C SAzymes and varying the reaction pH and temperature. The oxidase-like catalysis activity of Co–N–C SAzymes was concentration-dependent (Fig. 3b). By changing the pH from 2 to 9, the oxidase-like activity increased first and then decreased. Thus, pH 3 was selected as the optimum pH for further study (Fig. 3c). Co–N–C SAzymes maintained a high oxidase-like catalytic activity over the temperature

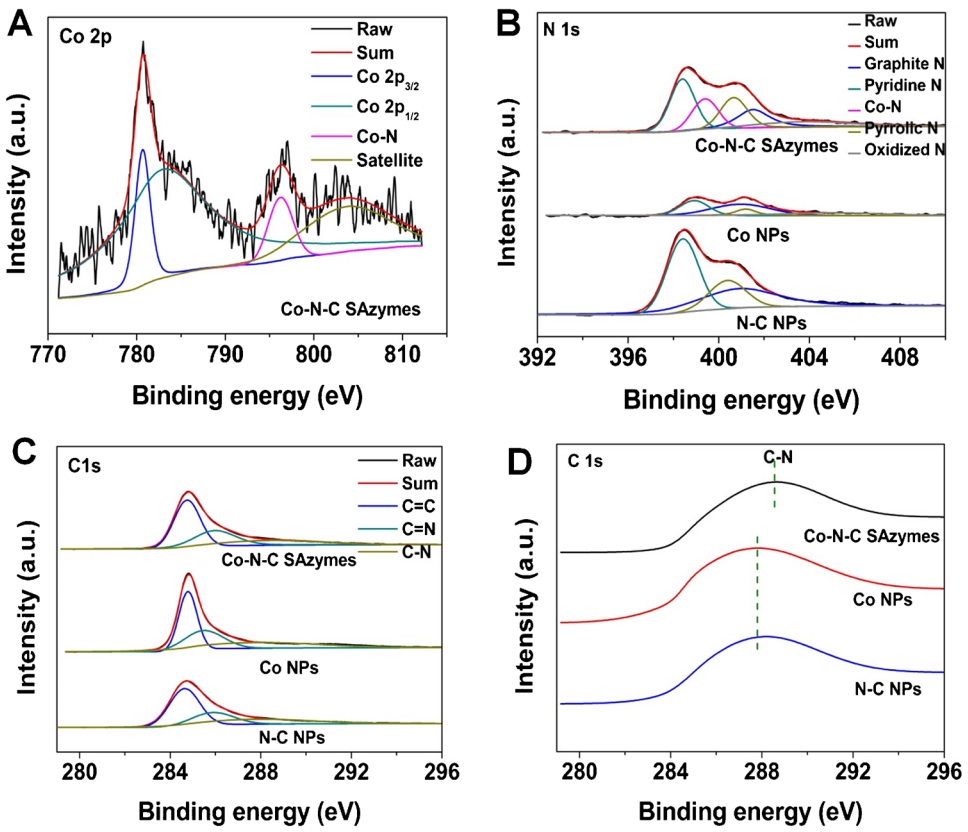

Fig. 2 **a** High-resolution XPS of Co 2*p* in Co–N–C SAzymes; (**b**) high-resolution XPS of N 1*s* in Co–N–C SAzymes, Co NPs, and N–C NPs; (**c**) high-resolution XPS of C 1*s* in Co–N–C SAzymes, Co NPs, and N–C NPs; (**d**) magnified image of the peak of C 1*s* assigned to C–N in (**c**)

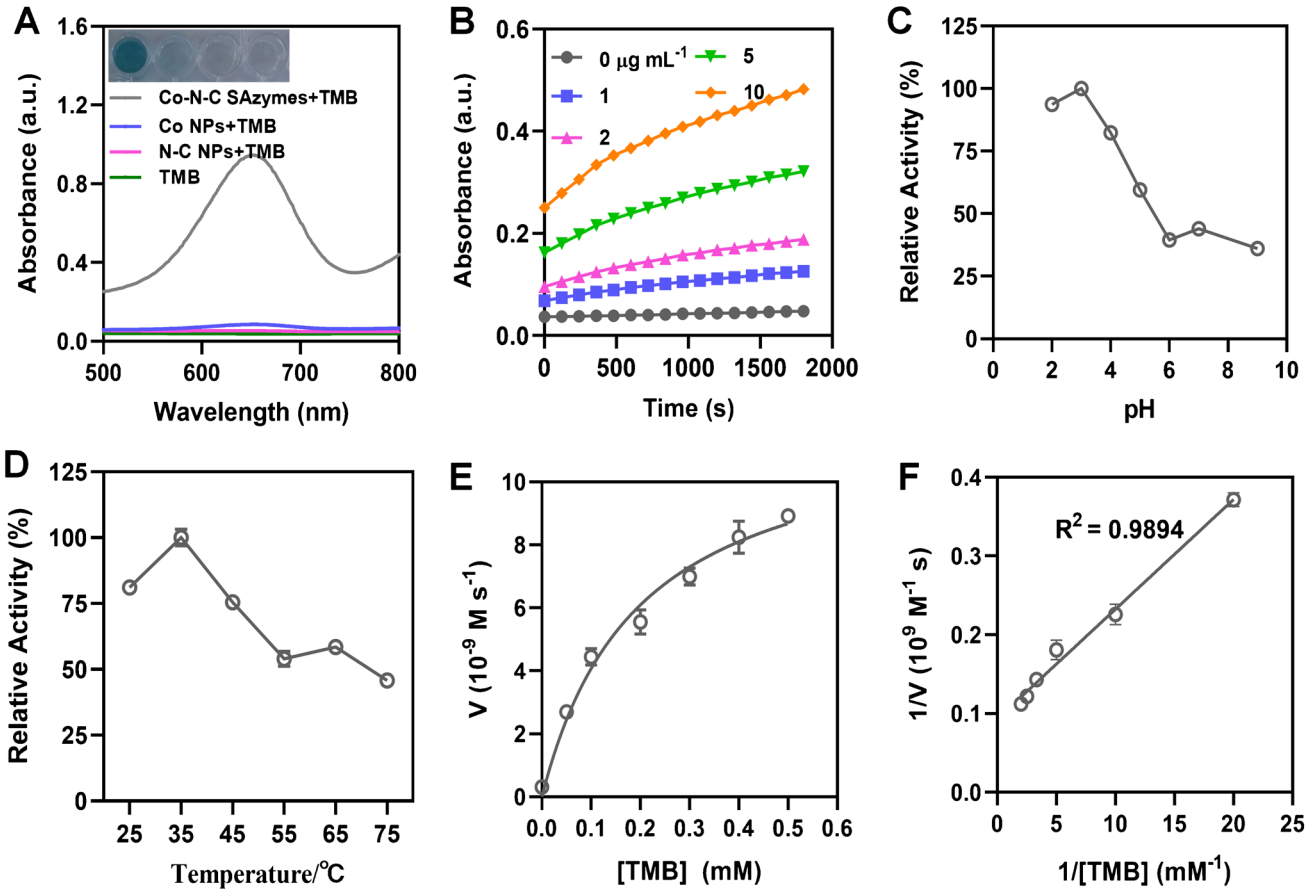

Fig. 3 **a** UV–Vis absorption spectra of Co–N–C SAzymes + TMB, Co NPs + TMB, N–C NPs + TMB, and TMB in HAc/NaAc buffer (20 mM, pH 3); (**b**) concentration-, (**c**) pH-, and (**d**) temperature-dependent oxidase-like activities of Co–N–C SAzymes; (**e**) steady-state kinetic assay; and (**f**) the corresponding Lineweaver–Burk plot of Co–N–C SAzymes for TMB

ranging from 25 to 45 °C, which retained 45.8% of their maximum activity even at 75 °C (Fig. 3d), indicating better temperature stability than natural enzymes.

To evaluate the enzyme kinetics of Co–N–C SAzymes, the typical Michaelis–Menten curves (Fig. 3e) and the corresponding Lineweaver–Burk plot were obtained (Fig. 3f). The Michaelis constant (K_m) and maximum reaction velocity (V_{max}) values are summarized in Table S1. Typically, the lower K_m value means stronger affinity between the enzyme and the substrate. The K_m value of Co–N–C SAzymes was lower than that of other nanozymes reported in the literature, indicating a high affinity of Co–N–C SAzymes toward TMB.

Detection of GSH/Cys with Co–N–C SAzymes

As Lewis bases, biothiols, such as GSH or Cys, tend to bind to Co single atoms and inhibit the oxidase-like activity. UV–Vis spectra of the reaction system before and after adding GSH/Cys were recorded (Fig. 4a). The absorbance of oxTMB decreased obviously after adding 50 μM GSH/Cys, which indicated the block of Co active sites of Co–N–C SAzymes. Besides, FTIR spectroscopy was employed to ensure the attachment of biothiols (Fig. 4b). For Cys-treated Co–N–C SAzymes, the new peak at 3000–3200 cm^{-1} confirmed the attachment of Cys on Co–N–C SAzymes. The disappearance of the thiols peak at around 2500 cm^{-1} was attributed to the coordination between S atoms of thiols and Co atoms of Co–N–C SAzymes. Furthermore, XPS of Cys and Co–N–C SAzymes/Cys were measured for investigating the electron density of S atoms (Figure S5). The S 2*p* peaks were seen to shift to a higher binding energy for about 0.8 eV, which further verified the strong coordination between Co atoms and thiols. The incubation time between GSH and Co–N–C SAzymes was optimized to achieve good detection performance, and the optimal incubation time was 15 min (Figure S6). UV–Vis absorbance spectra of Co–N–C SAzymes with various concentrations of GSH and the corresponding calibration plot are shown in Fig. 4c and d. The absorption peak at 652 nm decreased steadily with increasing the concentration of GSH from 0 to 100 μM (Fig. 4c), accompanied by color fading of the solution (the inserted photographs of Fig. 4d), which further demonstrated the

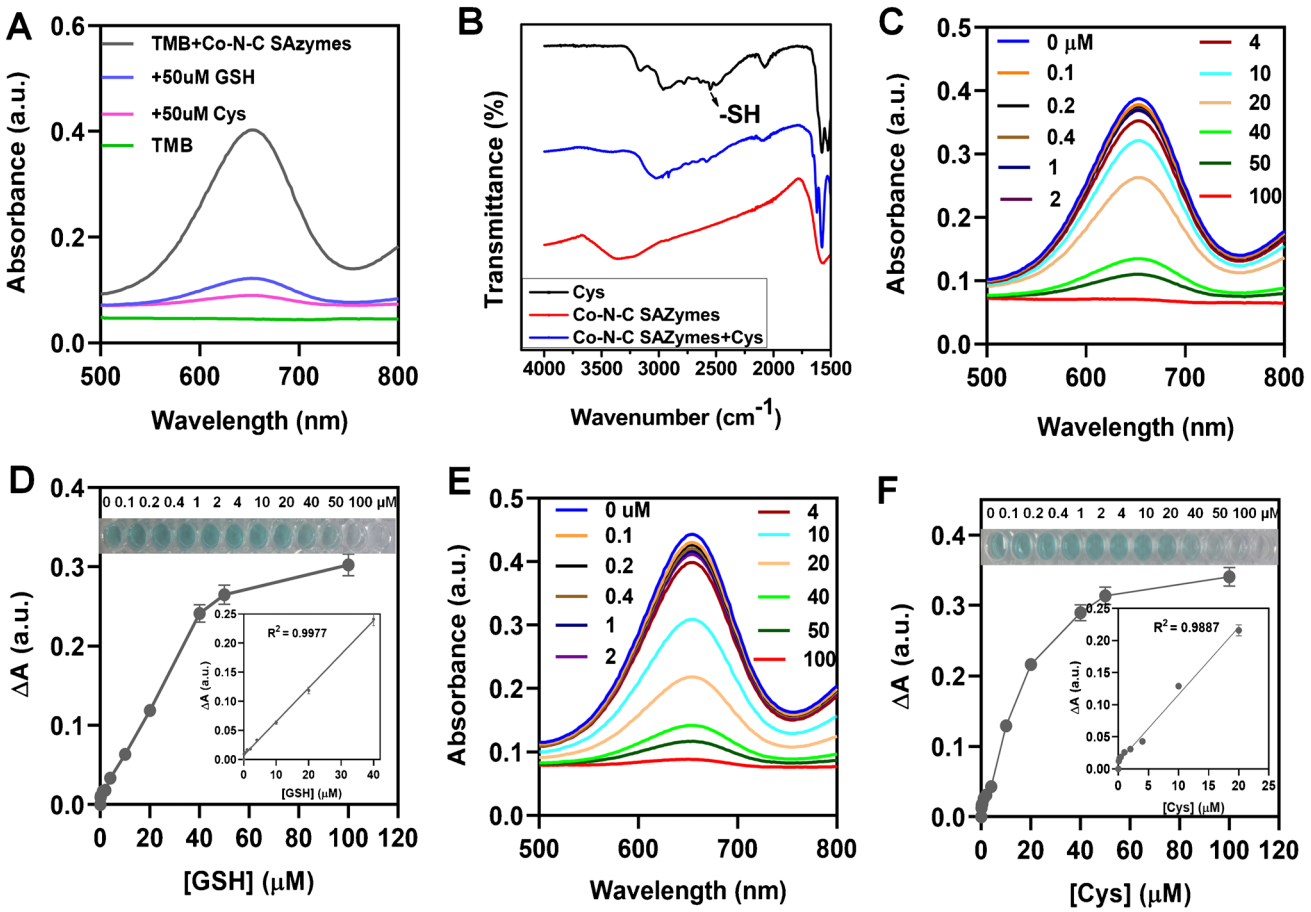

Fig. 4 **a** UV–Vis spectra of the interaction system (pH 3.0) formed by 250 μM TMB and 5 μg mL^{-1} Co–N–C SAzymes at 35 °C before and after adding 50 μM GSH/Cys; (**b**) FTIR spectra of the Co–N–C SAzymes, Cys-inhibited Co–N–C, and Cys; (**c**) UV–Vis spectra of the Co–N–C SAzymes/TMB system with various concentrations of GSH; (**d**) absorbance change ($\Delta A = A_0 - A$) and the linear calibration plot with increasing concentration of GSH. A and A_0 represent the absorbance value at 652 nm with and without GSH, respectively (the inset is the photographs of color changes for the corresponding concentrations of GSH); (**e**) UV–Vis spectra of the Co–N–C SAzymes/TMB system with various concentrations of Cys; (**f**) The absorbance change ($\Delta A = A_0 - A$) and the linear calibration plot with increasing concentration of Cys (the inset is the photographs of color changes for the corresponding concentrations of Cys)

inhibitory effect of GSH towards catalytic oxidation of TMB. Meanwhile, the absorbance difference $\Delta A = A_0 - A$ (A_0 and A represent the absorbance value at 652 nm in the absence and presence of GSH, respectively) and the linear calibration plot with increasing concentration of GSH were employed. The relationship between the absorbance difference and the concentration of GSH exhibited good linearity ($R^2 = 0.9977$) with the concentration ranging from 0.1 to 40 μM. The limit of detection (LOD) was calculated to be 0.07 μM by 3SD/slope. Similarly, UV–Vis absorbance spectra of Co–N–C SAzymes with various concentrations of Cys and the corresponding calibration plot are shown in Fig. 4e and f. The relationship between the absorbance difference and the concentration of Cys exhibited good linearity ($R^2 = 0.9887$) with the concentration ranging from 0.1 to 20 μM (LOD = 0.06 μM). By comparing the linear range and LOD of different nanozymes for colorimetric detection of GSH and Cys (Table S2), our sensing platform based on Co–N–C SAzymes showed a wider linear range and lower LOD, which indicated that Co–N–C SAzymes were superb probes.

In addition, the reproducibility of the GSH/Cys detection by Co–N–C SAzymes was evaluated (Fig. 5a), There were no significant differences in the absorbance difference of GSH/Cys among five repeated measurements, indicating good reproducibility. The specificity for GSH/Cys detection based on the proposed Co–N–C SAzyme colorimetric detection system was also evaluated by introducing 12 kinds of other amino acids (Leu, Ile, Asn, Ser, Trp, Thr, Ala, Val, Phe, Gly, Lys, and Glu) as interfering substances. The final concentration of GSH or Cys was 50 μM, and the concentration of other interfering substances was 500 μM. As can be seen from Fig. 5b, the ΔA value of the reaction system containing 50 μM GSH and Cys was much higher than that

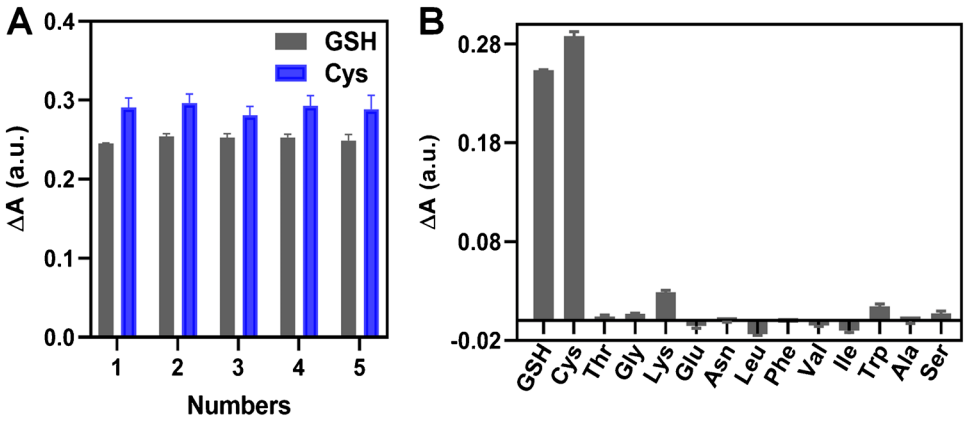

Fig. 5 **a** Reproducibility of GSH/Cys detection by Co–N–C SAzymes; (**b**) specificity analysis of GSH and Cys detection. The final concentration was 50 μM for GSH and Cys and 500 μM for other interfering substances

of other interfering substances with tenfold concentration, which showed that the developed Co–N–C SAzyme sensing platform could efficiently distinguish GSH and Cys from other amino acids and had excellent selectivity. FBS samples were use to investigate the feasibility of the proposed method for quantifying GSH in biological samples. Because the concentration of Cys in biological samples is far lower than that of GSH, the decreased absorbance value was approximately attributed to the concentration of GSH in FBS. The concentration of GSH in 10% FBS samples was measured to be 27.99 μM by our proposed method. Different concentrations of GSH were added into 10% FBS, and the total concentrations of GSH were measured by our approach. The obtained recoveries of spiked GSH in 10% FBS were between 97.03 and 101.68% (Table S3), indicating the developed Co–N–C SAzyme sensing platform could be used for detecting GSH in biological samples.

Conclusion

In summary, uniform Co–N–C SAzymes with excellent oxidase-like catalytic activity were successfully synthesized by a high-temperature pyrolysis approach. Biothiols, such as GSH or Cys, bind to Co single atoms and inhibit the oxidase-like activity, resulting in concentration-dependent color fading and absorbance decrease of the solution. Therefore, a sensitive and straightforward colorimetric platform based on the oxidase-like activity of Co–N–C SAzymes was developed for biothiol (GSH/Cys) detection. This proposed method is very simple and low-cost. The detection limit was 0.07 μM for GSH and 0.06 μM for Cys. Additionally, the method showed good reproducibility and high selectivity against other amino acids. This work broadened the application of Co–N–C SAzymes in the biosensing field.

Supplementary Information The online version contains supplementary material available at https://doi.org/10.1007/s00216-021-03816-4.

Acknowledgements This work was supported by the National Natural Science Foundation of China (Grant 31971314), the Distinguished Youth Foundation of Anhui Province (1808085J05), the Fundamental Research Funds for the Central Universities of China (Grant No. JZ2017HGPA0164, JZ2021HGTB0120), and the Key research and development plan of Anhui Province (202104b11020015).

Author contribution Liping Sun and Yong Yan designed the project, carried out experiments, analyzed the data, and wrote the original draft. Shuai Chen, Zijue Zhou, and Wei Tao analyzed the data, discussed the results, and read the final manuscript. Chao Li, Yi Feng, and Feng Wang supervised the project, gave suggestions to revise the manuscript, and provided financial support.

Declarations

Competing interest There are no conflicts of interest to declare.

References

1. Liu W, Chen J, Xu Z. Fluorescent probes for biothiols based on metal complex. Coordin Chem Rev. 2021;429:213638.
2. Zhang L, Cai QY, Li J, Ge J, Wang JY, Dong ZZ, Li ZH. A label-free method for detecting biothiols based on poly(thymine)-templated copper nanoparticles. Biosens Bioelectron. 2015;69:77–82.
3. Huang M, Wang H, He D, Jiang P, Zhang Y. Ultrafine and monodispersed iridium nanoparticles supported on nitrogen-functionalized carbon: an efficient oxidase mimic for glutathione colorimetric detection. Chem Commun. 2019;55(25):3634–7.
4. Zhang X, Mao X, Li S, Dong W, Huang Y. Tuning the oxidase mimics activity of manganese oxides via control of their growth conditions for highly sensitive detection of glutathione. Sens Actuators B Chem. 2018;258:80–7.
5. Li X, Yang XY, Sha JQ, Han T, Du CJ, Sun YJ, Lan YQ. POMOF/SWNT nanocomposites with prominent peroxidase-mimicking activity for L-Cysteine "on-off switch" colorimetric biosensing. ACS Appl Mater Interfaces. 2019;11(18):16896–904.
6. Wang F, Zhu Y, Xu J, Xu Z, Cheng G, Zhang W. Highly selective and ratiometric fluorescent nanoprobe for the detection of cysteine and its application in test strips. Anal Bioanal Chem. 2018;410(20):4875–84.
7. Allocati N, Masulli M, Di Ilio C, Federici L. Glutathione transferases: substrates, inihibitors and pro-drugs in cancer and neurodegenerative diseases. Oncogenesis. 2018;7(1):8.

8. Ozyurek M, Baki S, Gungor N, Celik SE, Guclu K, Apak R. Determination of biothiols by a novel on-line HPLC-DTNB assay with post-column detection. Anal Chim Acta. 2012;750:173–81.
9. Isokawa M, Funatsu T, Tsunoda M. Fast and simultaneous analysis of biothiols by high-performance liquid chromatography with fluorescence detection under hydrophilic interaction chromatography conditions. Analyst. 2013;138(13):3802–8.
10. Liu Z, Liu Y, Kim E, Bentley WE, Payne GF. Electrochemical probing through a redox capacitor to acquire chemical information on biothiols. Anal Chem. 2016;88(14):7213–21.
11. Pang X, Bai H, Xu D, Ding J, Fan W, Shi W. Dual-functional electrochemical bio-sensor built from Cu2O for sensitively detecting the thiols and Hg^{2+}. Appl Surf Sci. 2021;564:150397.
12. Pang X, Bai H, Zhao H, Liu Y, Qin F, Han X, Fan W, Shi W. Biothiol-functionalized cuprous oxide sensor for dual-mode sensitive Hg^{2+} detection. ACS Appl Mater Interfaces. 2021;13(39):46980–9.
13. Zhang B, Zhang H, Zhong M, Wang S, Xu Q, Cho D-H, Qiu H. A novel off-on fluorescent probe for specific detection and imaging of cysteine in live cells and in vivo. Chin Chem Lett. 2020;31(1):133–5.
14. Cai QY, Li J, Ge J, Zhang L, Hu YL, Li ZH, Qu LB. A rapid fluorescence "switch-on" assay for glutathione detection by using carbon dots-MnO_2 nanocomposites. Biosens Bioelectron. 2015;72:31–6.
15. Sheng Z, Chen L. Switch-on fluorescent strategy based on crystal violet-functionalized CdTe quantum dots for detecting L-cysteine and glutathione in water and urine. Anal Bioanal Chem. 2017;409(26):6081–90.
16. Ge J, Cai R, Chen X, Wu Q, Zhang L, Jiang Y, Cui C, Wan S, Tan W. Facile approach to prepare HSA-templated MnO_2 nanosheets as oxidase mimic for colorimetric detection of glutathione. Talanta. 2019;195:40–5.
17. Xue H, Yu M, He K, Liu Y, Cao Y, Shui Y, Li J, Farooq M, Wang L. A novel colorimetric and fluorometric probe for biothiols based on MnO_2 NFs-Rhodamine B system. Anal Chim Acta. 2020;1127:39–48.
18. Munyemana JC, Chen J, Wei X, Ali MC, Han Y, Qiu H. Deep eutectic solvent-assisted facile synthesis of copper hydroxide nitrate nanosheets as recyclable enzyme-mimicking colorimetric sensor of biothiols. Anal Bioanal Chem. 2020;412(19):4629–38.
19. Liu J, Meng L, Fei Z, Dyson PJ, Jing X, Liu X. MnO_2 nanosheets as an artificial enzyme to mimic oxidase for rapid and sensitive detection of glutathione. Biosens Bioelectron. 2017;90:69–74.
20. Hou J, Jia P, Yang K, Bu T, Sun X, Wang L. Facile preparation of Ru@V_2O_4 nanowires exhibiting excellent tetra-enzyme mimetic activities for sensitive colorimetric H_2O_2 and cysteine sensing. Sens Actuators B Chem. 2021;344:130266.
21. Chen Y, Chen T, Wu X, Yang G. $CuMnO_2$ nanoflakes as pH-switchable catalysts with multiple enzyme-like activities for cysteine detection. Sens Actuators B Chem. 2019;279:374–84.
22. Ma W, Mao J, Yang X, Pan C, Chen W, Wang M, Yu P, Mao L, Li Y. A single-atom Fe-N4 catalytic site mimicking bifunctional antioxidative enzymes for oxidative stress cytoprotection. Chem Commun. 2018;55(2):159–62.
23. Pei JH, Zhao RL, Mu XY, Wang JY, Liu CL, Zhang XD. Single-atom nanozymes for biological applications. Biomater Sci. 2020;8(23):6428–41.
24. Jiao L, Xu WQ, Yan HY, Wu Y, Liu CR, Du D, Lin YH, Zhu CZ. Fe-N-C Single-atom nanozymes for the intracellular hydrogen peroxide detection. Anal Chem. 2019;91(18):11994–9.
25. Cheng N, Li JC, Liu D, Lin Y, Du D. Single-atom nanozyme based on nanoengineered Fe-N-C catalyst with superior peroxidase-like activity for ultrasensitive bioassays. Small. 2019;15(48):e1901485.
26. Mao Y, Gao S, Yao L, Wang L, Qu H, Wu Y, Chen Y, Zheng L. Single-atom nanozyme enabled fast and highly sensitive colorimetric detection of Cr(VI). J Hazard Mater. 2021;408:124898.
27. Zhou X, Wang M, Chen J, Xie X, Su X. Peroxidase-like activity of Fe-N-C single-atom nanozyme based colorimetric detection of galactose. Anal Chim Acta. 2020;1128:72–9.
28. Chen Q, Li S, Liu Y, Zhang X, Tang Y, Chai H, Huang Y. Size-controllable Fe-N/C single-atom nanozyme with exceptional oxidase-like activity for sensitive detection of alkaline phosphatase. Sens Actuators B Chem. 2020;305:127511.
29. Jiao L, Xu W, Zhang Y, Wu Y, Gu W, Ge X, Chen B, Zhu C, Guo S. Boron-doped Fe-N-C single-atom nanozymes specifically boost peroxidase-like activity. Nano Today. 2020;35:100971.
30. Niu X, Shi Q, Zhu W, Liu D, Tian H, Fu S, Cheng N, Li S, Smith JN, Du D, Lin Y. Unprecedented peroxidase-mimicking activity of single-atom nanozyme with atomically dispersed Fe-Nx moieties hosted by MOF derived porous carbon. Biosens Bioelectron. 2019;142:111495.
31. Cao F, Zhang L, You Y, Zheng L, Ren J, Qu X. An Enzyme-Mimicking Single-atom catalyst as an efficient multiple reactive oxygen and nitrogen species scavenger for sepsis management. Angew Chem Int Ed. 2020;59(13):5108–15.
32. Yin P, Yao T, Wu Y, Zheng L, Lin Y, Liu W, Ju H, Zhu J, Hong X, Deng Z, Zhou G, Wei S, Li Y. Single cobalt atoms with precise N-coordination as superior oxygen reduction reaction catalysts. Angew Chem Int Ed. 2016;55(36):10800–5.